

Article

Enhanced Thermoelectric Properties of Graphene/Cu₂SnSe₃ Composites

Degang Zhao *, Xuezheng Wang and Di Wu

School of Materials Science and Engineering, University of Jinan, Jinan 250022, China; ujn_wangxz@yeah.net (X.W.); crystal4885@sina.com (D.W.)

* Correspondence: mse_zhaodg@ujn.edu.cn; Tel.: +86-531-8276-7561

Academic Editor: George S. Nolas

Received: 28 January 2017; Accepted: 27 February 2017; Published: 28 February 2017

Abstract: Cu₂SnSe₃ material is regarded as a potential thermoelectric material due to its relatively high carrier mobility and low thermal conductivity. In this study, graphene was introduced into the Cu₂SnSe₃ powder by ball milling, and the bulk graphene/Cu₂SnSe₃ thermoelectric composites were prepared by spark plasma sintering. The graphene nanosheets distributed uniformly in the Cu₂SnSe₃ matrix. Meanwhile, some graphene nanosheets tended to form thick aggregations, and the average length of these aggregations was about 3 μm. With the fraction of graphene increasing, the electrical conductivity of graphene/Cu₂SnSe₃ samples increased greatly while the Seebeck coefficient was decreased. The introduction of graphene nanosheets can reduce the thermal conductivity effectively resulting from the phonon scattering by the graphene interface. When the content of graphene exceeds a certain value, the thermal conductivity of graphene/Cu₂SnSe₃ composites starts to increase. The achieved highest figure of merit (*ZT*) for 0.25 vol % graphene/Cu₂SnSe₃ composite was 0.44 at 700 K.

Keywords: thermoelectric; composites; ternary diamond-like semiconductor; graphene

1. Introduction

Due to the dilemma between energy crisis and environmental stewardship, developing renewable energy technologies has attracted considerable research interest in the past decade. Thermoelectric materials, which can directly convert heat energy into electrical energy and vice versa, show great promise in the application of solid-state cooling, waste heat recovery, and power generation. The conversion efficiency of thermoelectric material is governed by the dimensionless figure of merit, $ZT = \sigma\alpha^2T/\kappa$, where σ , α , T , and κ are the electrical conductivity, Seebeck coefficient, absolute temperature and thermal conductivity, respectively. The total thermal conductivity is composed of carrier thermal conductivity (κ_c) and lattice thermal conductivity (κ_l). Therefore, thermoelectric materials with good performance should have a large α and σ and low κ . As the fundamental material parameters (α , σ , and κ_c) are interrelated and conflicting via carrier concentration in bulk thermoelectric materials, it is a longstanding challenge to largely improve the overall *ZT* [1–4]. Therefore, concepts or strategies that can decouple these parameters to simultaneously optimize the electron and phonon transport are highly encouraging and imperative for the thermoelectric community. Specifically, band engineering and nanostructuring have been demonstrated as effective extrinsic approaches to separately enhance the power factor ($PF = \alpha^2\sigma$) and reduce the κ_l , respectively.

Several classes of thermoelectric materials, such as skutterudite [5,6], tellurides [7–10], half-Heuslers [11,12], and silicides [13,14], have been modified to reach high *ZT* value. Recently, ternary diamond-like semiconductor of Cu₂SnSe₃ has emerged as a new potential thermoelectric material due to its relatively high carrier mobility and quite low thermal conductivity. Since the Cu–Se bond network in the Cu₂SnSe₃ structure forms an electrically conductive framework and Sn orbitals contribute little to the carrier transport, the electrical conductivity of Cu₂SnSe₃ is allowed to be tuned

to optimize the thermoelectric property by partial substitution of the Sn site. Some valuable work has been done on Cu_2SnSe_3 compound by doping, substitution, or solid solution [15,16]. The In-doped $\text{Cu}_2\text{In}_x\text{Sn}_{1-x}\text{Se}_3$ was studied by Chen et al. and a maximum ZT of around 1.2 was obtained at 850 K for $x = 0.1$ [17]. Similarly, gallium doping was found to be an effective way to increase the ZT in Ga-doped Cu_2SnSe_3 compounds by Shi et al., and the maximum ZT increased to 0.43 at 700 K [18]. Moreover, isoelectronic alloying with Ge at the Sn site was confirmed to be effective in enhancing the ZT value by Morelli et al. [19]. Besides substitution, the introduction of a nanostructure phase into the matrix is also an attractive approach to enhance the dimensionless figure of merit of thermoelectric materials. So far, there are few studies about nanostructured Cu_2SnSe_3 matrix composites due to the unapparent enhancement of ZT resulting from the second nanostructured phase. Although a remarkable decrease in the lattice conductivity can be achieved by phonon scattering at nanophase/matrix interfaces, the electrical properties of thermoelectric composites also decrease, leading to a marginal change of the overall ZT value. Moreover, the selection of nanophase and the control of the microstructure of thermoelectric composites are also important for the enhancement of ZT value [20–22].

Graphene has high electrical and thermal properties due to its unique 2D structure. The carrier mobility, electrical conductivity, and thermal conductivity of graphene is $2 \times 10^5 \text{ cm}^2 \cdot \text{V}^{-1} \cdot \text{s}^{-1}$, $1 \times 10^6 \text{ S/m}$, and $5 \times 10^3 \text{ Wm}^{-1} \cdot \text{K}^{-1}$ at room temperature, respectively. Meanwhile, the carrier of graphene with zero bandgap can continuously vary from electron to hole, which can benefit the electrical transport in the p–n interfacial region. Wang et al. even confirmed that the introduction of 0.2 vol % graphene enhanced the ZT value of Bi_2Te_3 material [23]. Kim et al. confirmed that the peak ZT value for the 0.05 wt % graphene/ $\text{Bi}_2\text{Te}_{2.7}\text{Se}_{0.3}$ composite increased to 0.8 at 400 K, which is 23% larger than that of the pristine sample [24]. Chen et al. also showed that an improved ZT value of 0.4 in graphene/ CuInTe_2 composites was obtained due to a lower κ_1 [25]. In this contribution, it is highly possible that incorporating graphene nanosheets into Cu_2SnSe_3 material will also lead to reduced κ_1 , which perhaps will further improve the thermoelectric properties of graphene/ Cu_2SnSe_3 composites.

In the present work, graphene nanosheets were incorporated into the Cu_2SnSe_3 matrix by ball-milling method, and the graphene/ Cu_2SnSe_3 thermoelectric composites were fabricated by spark plasma sintering (SPS). The transport properties of graphene/ Cu_2SnSe_3 composites were studied with the aim of enhancing thermoelectric performance of Cu_2SnSe_3 .

2. Experimental Procedures

Cu_2SnSe_3 was synthesized by the reacting stoichiometric copper (powder, 99.96%), tin (powder, 99.999%), and selenium (shot, 99.999%) in evacuated fused-silica ampoules at 1173 K for 12 h, then slowly cooling the melt down to 873 K for 24 h, followed by annealing at this temperature for 2 days. Finally, the obtained ingots were reground into fine powder. Commercially available graphene powder (single layer, average diameter: 2 μm , thickness: 0.8 nm; XFNANO, Nanjing, China) was chosen as the second nanophase, just as shown in Figure 1. The graphene powder was incorporated into the Cu_2SnSe_3 powder at volume fractions of 0.25, 0.50, 0.75, and 1.0 vol %, respectively. Then, the graphene-added Cu_2SnSe_3 powders were mechanically milled with a planetary ball-milling machine. The ball-to-powder ratio was 5:1, and the ball-milling process was carried out in Ar atmosphere for 240 min at 150 rpm. The SPS process was used to consolidate the as-milled powders at 860 K for 8 min in a vacuum of 0.1 Pa under a pressure of 50 MPa.

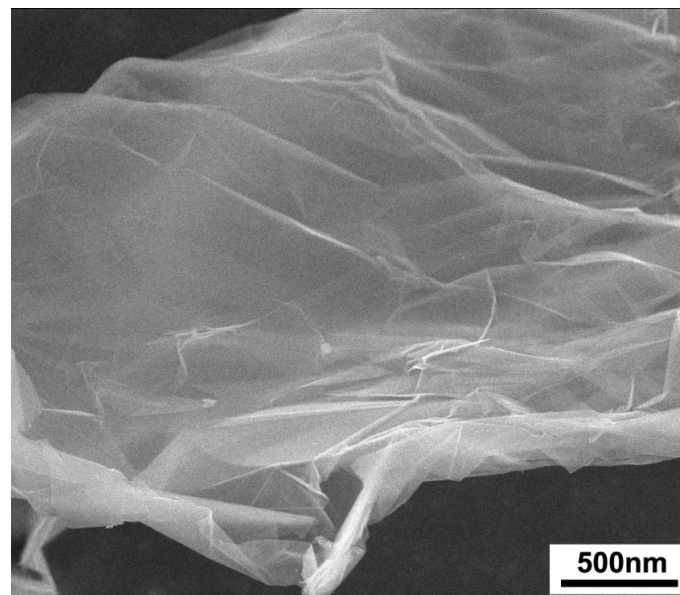


Figure 1. SEM image of single-layer graphene with an average diameter of 2 μm .

The constituent phases of the samples were characterized by X-ray diffractometry on a Rigaku Rint2000 powder diffractometer equipped with Cu K_{α} radiation. The microstructure of all graphene/ Cu_2SnSe_3 samples was observed using field-emission scanning electron microscopy (FESEM) and high-resolution transmission electron microscopy (HRTEM, JEM2100F, JEOL, Tokyo, Japan). The thermal diffusivity (λ) of all samples was measured on the disk-shaped specimen by laser flash technique using a Netzsch LFA427 (Netzsch, Berlin, German) setup in a flowing Ar atmosphere with temperature ranging from 300 to 700 K. The thermal conductivity was then calculated as $\kappa = d\lambda C_p$, where d is the density measured by Archimedes method, and C_p is the Dulong–Petit approximation for the specific heat capacity. A bar-shaped specimen of $2 \times 2 \times 10 \text{ mm}^3$ was cut with a diamond saw from the sample for the measurement of electrical transport properties. Both electrical conductivity and Seebeck coefficient were determined simultaneously using ZEM-3 equipment (ULVAC-RIKO, Tokyo, Japan) with temperature ranging from 300 to 700 K in Ar atmosphere. The Hall coefficients (R_H) were measured by van der Pauw’s method in a vacuum of 0.1 Pa under a magnetic field of 2 T. The carrier mobility (μ_H) and carrier concentration (p) were calculated through the formulae of $\mu_H = R_H\sigma$ and $p_H = 1/(R_He)$ based on the assumption of single-band model, where e is the electron charge. The experimental uncertainty on the electrical conductivity, Seebeck coefficient, thermal conductivity, and Hall coefficient are estimated to be 5%, 5%, 8%, and 4%, respectively.

3. Results and Discussion

3.1. Phase Analysis and Microstructure

Figure 2 displays the SEM image of the 1.0 vol % graphene-added Cu_2SnSe_3 powder after ball milling for 240 min at 150 rpm. It can be observed that the average diameter of graphene nanosheets in the mixed Cu_2SnSe_3 powder was about 1 μm . Figure 3 is the X-ray diffraction patterns of sintered graphene/ Cu_2SnSe_3 composites. The diffraction peaks in Figure 3 are identified as JCPDS card 65-4145 (cubic Cu_2SnSe_3). No diffraction peak of graphene is found in the XRD results as the fraction of graphene in the composites is very low. All graphene/ Cu_2SnSe_3 composites show the same XRD patterns as the pristine Cu_2SnSe_3 .

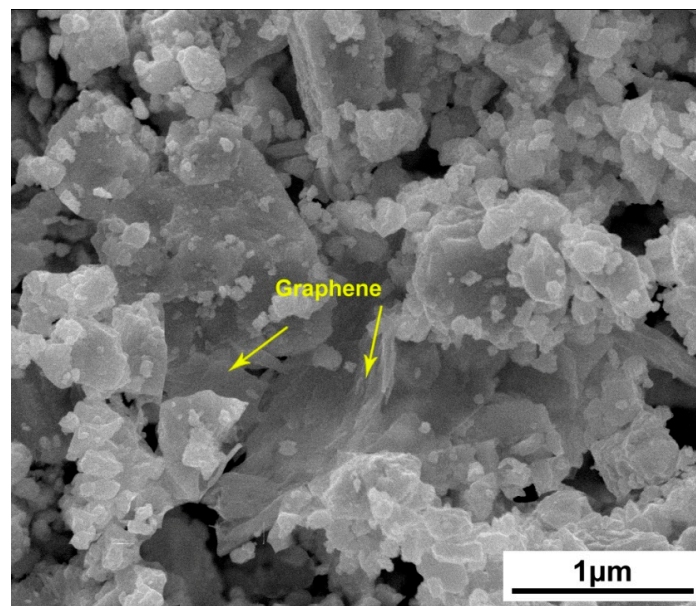


Figure 2. SEM image of the 1.0 vol % graphene/ Cu_2SnSe_3 powder after ball milling.

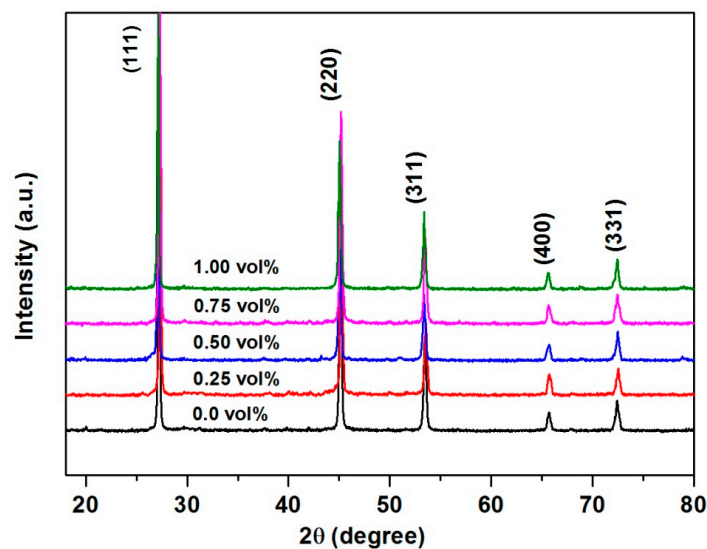


Figure 3. XRD patterns of sintered graphene/ Cu_2SnSe_3 samples.

The microstructure of the sintered pristine Cu_2SnSe_3 and 0.75 vol % graphene/ Cu_2SnSe_3 sample is illustrated in Figure 4a,b, respectively. It is evident that the graphene nanosheets distributed uniformly in the Cu_2SnSe_3 matrix. Meanwhile, some graphene nanosheets tended to form thick aggregations and the average length of aggregations was about 3 μm . A similar phenomenon was also observed by Zhao et al. in the graphene/ CoSb_3 nanocomposite [26]. The results of energy dispersive X-ray spectroscopy (EDS) for graphene/ Cu_2SnSe_3 sample identify that the matrix consisted of 33.17 atom % copper, 16.79 atom % tin, and 50.04 atom % selenium, indicating the Cu_2SnSe_3 phase, just as shown in Figure 5. The black phase in Figure 5a only contains the C element, corresponding to the graphene phase. It can be observed from HRTEM in Figure 6 that most of the graphene nanosheets is of the multilayered form (<10 layers), which is consistent with SEM results. The fringe spacing of 0.81 nm in the lattice image corresponds to the interplanar distance of the (111) plane of Cu_2SnSe_3 . Figure 7 shows the FESEM image of the fractured surface of the sintered graphene/ Cu_2SnSe_3 sample. The graphene nanosheets are homogeneously embedded in the Cu_2SnSe_3 matrix. According to the classic band

theory [27,28], nanostructures distributed in the material can result in strain fields, then lead to a change in the energy-band structure of thermoelectric material. At the same time, nanophases can greatly influence the phonon and electronic transport of thermoelectric materials.

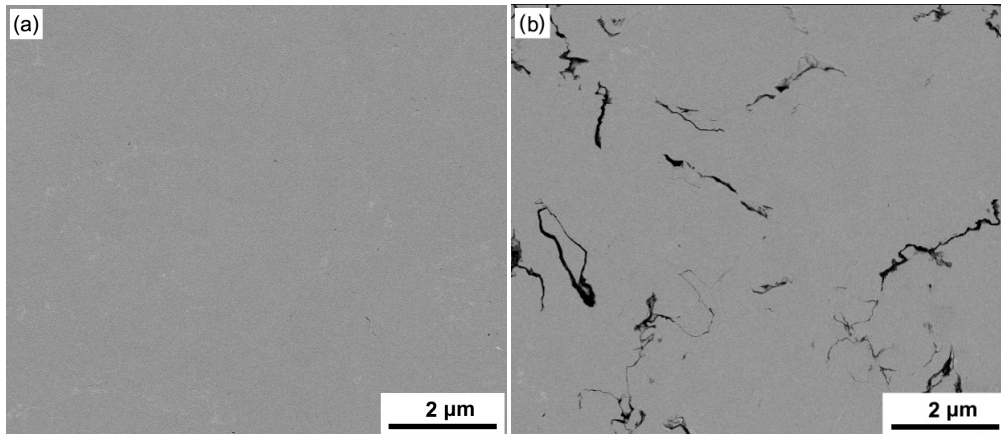


Figure 4. SEM image of the sintered (a) Cu_2SnSe_3 ; (b) 0.75 vol % graphene/ Cu_2SnSe_3 sample.

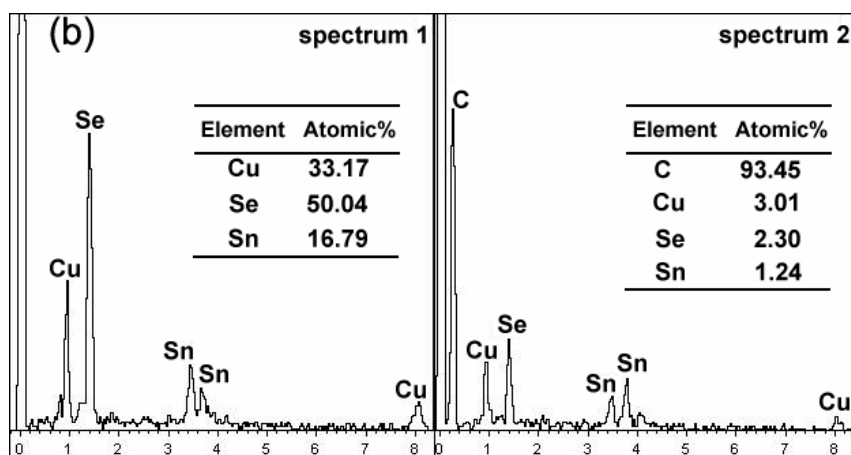
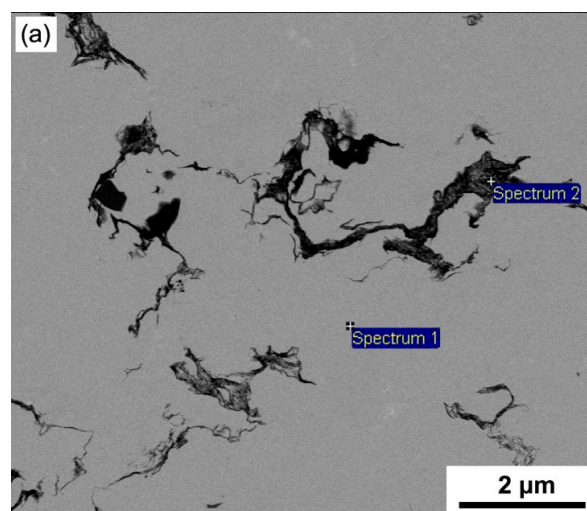


Figure 5. (a) SEM image of the sintered 1.0% graphene/ Cu_2SnSe_3 composite; (b) energy dispersive X-ray spectroscopy (EDS) analysis.

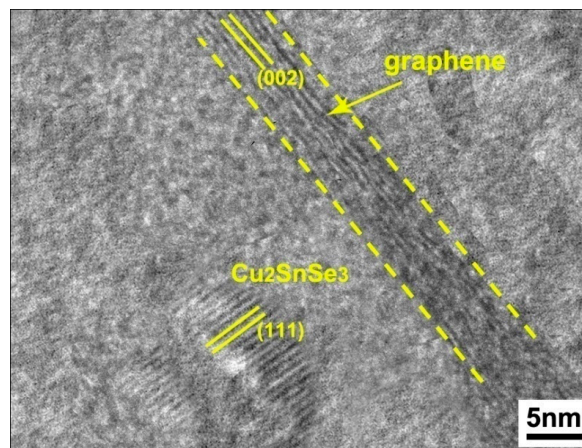


Figure 6. High-resolution TEM (HRTEM) image of graphene nanosheets in the graphene/ Cu_2SnSe_3 sample.

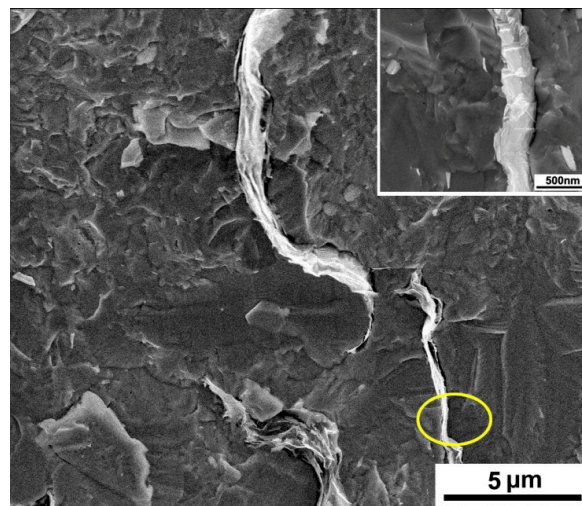


Figure 7. Field-emission SEM (FESEM) image of fractured surface of the sintered graphene/ Cu_2SnSe_3 sample.

3.2. Electrical Properties

Figure 8 presents the σ of graphene/ Cu_2SnSe_3 composites as a function of temperature. It can be observed that the σ of the pristine Cu_2SnSe_3 sample declines steeply with the temperature increasing across the overall temperature range, showing a typical heavily doped degenerate semiconducting behavior. It is noteworthy that graphene/ Cu_2SnSe_3 samples show an obvious increased σ compared with pristine Cu_2SnSe_3 due to the introduction of conductivity graphene nanosheets. In addition, the σ of graphene/ Cu_2SnSe_3 samples increases with the increasing fraction of graphene. The σ of 1.0 vol % graphene/ Cu_2SnSe_3 sample at room temperature is about $350 \Omega^{-1}\cdot\text{cm}^{-1}$, which is about 3 times the value of the pristine Cu_2SnSe_3 . Even at the high-temperature region, the σ of graphene/ Cu_2SnSe_3 sample still retains a high value. The σ of 0.25 vol % graphene/ Cu_2SnSe_3 sample is around $124 \Omega^{-1}\cdot\text{cm}^{-1}$ at 700 K. The enhancement in σ for graphene/ Cu_2SnSe_3 samples may be ascribed to either an increase of carrier concentration (p), or the increment in carrier mobility (μ_H), or both. Table 1 lists some physical and structural parameters of the graphene/ Cu_2SnSe_3 composites at room temperature. As shown in Table 1, the carrier concentration of graphene/ Cu_2SnSe_3 composites is higher than that of pristine Cu_2SnSe_3 . The carrier mobility increases from $21.2 \text{ cm}^2/\text{V}\cdot\text{s}$ for Cu_2SnSe_3 to $34.3 \text{ cm}^2/\text{V}\cdot\text{s}$ for the 1.0 vol % graphene/ Cu_2SnSe_3 sample. Therefore, it can be concluded that incorporating graphene nanosheets into a Cu_2SnSe_3 matrix can improve the electrical conductivity, which is attributed to the increment in both carrier concentration and mobility. This is reasonable

because the multilayered graphene is *p*-type thermoelectric material, and the graphene itself can afford the charged carrier [29]. In addition, the graphene has a relatively high mobility, which is beneficial to increase the carrier mobility of graphene/Cu₂SnSe₃ composites.

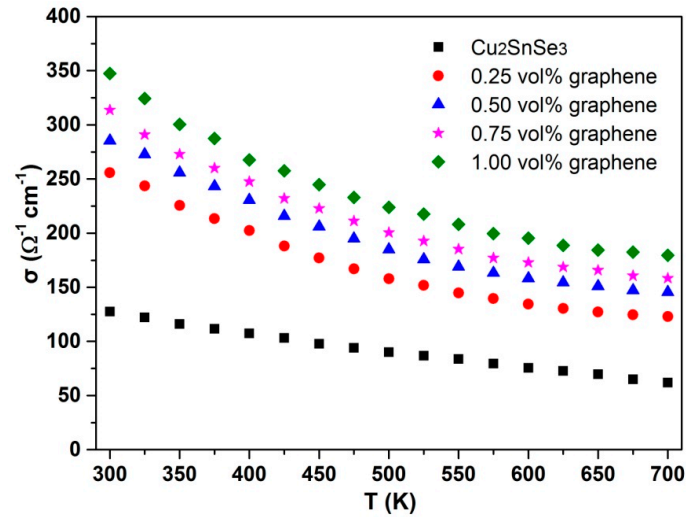


Figure 8. Electrical conductivity of graphene/Cu₂SnSe₃ samples as a function of temperature.

Table 1. Chemical composition and some physical and structural parameters of graphene/Cu₂SnSe₃ composites at room temperature.

<i>x</i> (vol %)	Relative Density	σ ($\Omega^{-1}\cdot\text{cm}^{-1}$)	p (10^{19} cm^{-3})	μ_{H} ($\text{cm}^2/\text{V}\cdot\text{s}$)	α ($\mu\text{V}/\text{K}$)	κ_1 ($\text{W}\cdot\text{m}^{-1}\cdot\text{K}^{-1}$)	m^* (m_0)
0	98.7%	127	3.74	21.2	131	2.65	2.6
0.25	98.1%	255	5.43	29.3	99.8	2.36	2.8
0.50	98.0%	285	5.86	30.4	92.0	2.59	2.9
0.75	97.8%	313	6.13	31.9	78.7	2.92	2.7
1.00	97.5%	448	8.16	34.3	69.9	3.24	3.1

x: volume fraction; σ : electrical conductivity; p : charge carrier concentration; μ_{H} : carrier mobility; α : Seebeck coefficient; κ_1 : thermal conductivity; m^* : density of states effective mass

Figure 9 demonstrates the α of graphene/Cu₂SnSe₃ samples as a function of temperature. It can be seen that the α of all graphene/Cu₂SnSe₃ samples across the whole temperature range was positive, indicating the major charge carriers in the samples are holes. Moreover, the α of all graphene/Cu₂SnSe₃ composites and pristine Cu₂SnSe₃ samples increases approximately linearly with increasing temperature. For example, the α of pristine Cu₂SnSe₃ increases from 130 $\mu\text{V}/\text{K}$ to 255 $\mu\text{V}/\text{K}$ in the temperature range of 300–700 K. At the same time, the introduction of graphene nanosheets decreased the Seebeck coefficients of Cu₂SnSe₃ samples evidently. Compared with the α of pristine Cu₂SnSe₃ sample, the α of graphene/Cu₂SnSe₃ samples decreases with the increasing fraction of graphene. At room temperature, the α decreases from 130 $\mu\text{V}/\text{K}$ for Cu₂SnSe₃ matrix to 70 $\mu\text{V}/\text{K}$ for the 1.0% graphene/Cu₂SnSe₃ composite. The decrease of α for graphene/Cu₂SnSe₃ composites can be explained by the equation

$$\alpha = \pm \frac{k_{\text{B}}}{e} \left[2 + \ln \frac{2(2\pi m^* k_{\text{B}} T)^{\frac{3}{2}}}{h^3 p} \right] \quad (1)$$

where k_{B} , m^* , h , and p are Boltzmann constant, density of states effective mass, Planck's constant, and charge carrier concentration, respectively. The introduction of graphene nanosheets leads to the improved carrier density. Herein, according to the equation, the α is reduced.

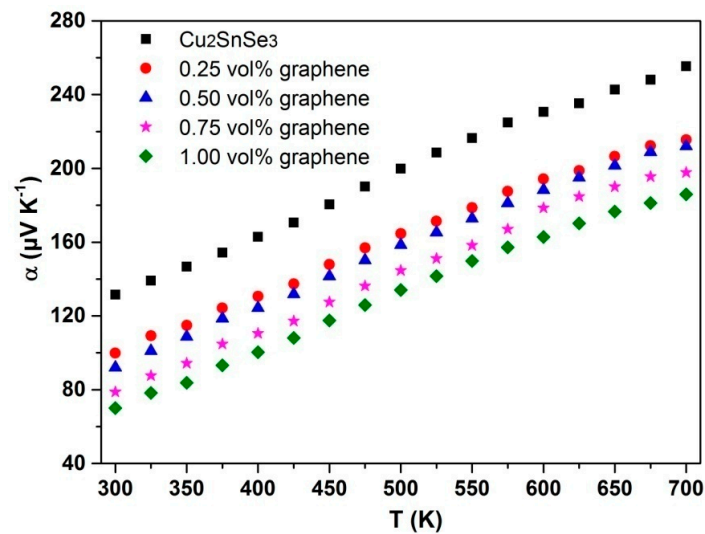


Figure 9. Seebeck coefficient (α) of graphene/ Cu_2SnSe_3 samples as a function of temperature.

The μ_{H} of graphene/ Cu_2SnSe_3 composites as a function of temperature is displayed in Figure 10. The μ_{H} of graphene/ Cu_2SnSe_3 composites increases with the increasing fraction of graphene. Moreover, the μ_{H} of graphene/ Cu_2SnSe_3 samples in this study is between 20 and 35 $\text{cm}^2 \cdot \text{V}^{-1} \cdot \text{s}^{-1}$ at room temperature, which is close with that of CoSb_3 [30,31]. This may be attributed to the similar carrier effective mass (m^*) of Cu_2SnSe_3 and skutterudite compounds. The m^* can be calculated by the following equations based on single parabolic band model.

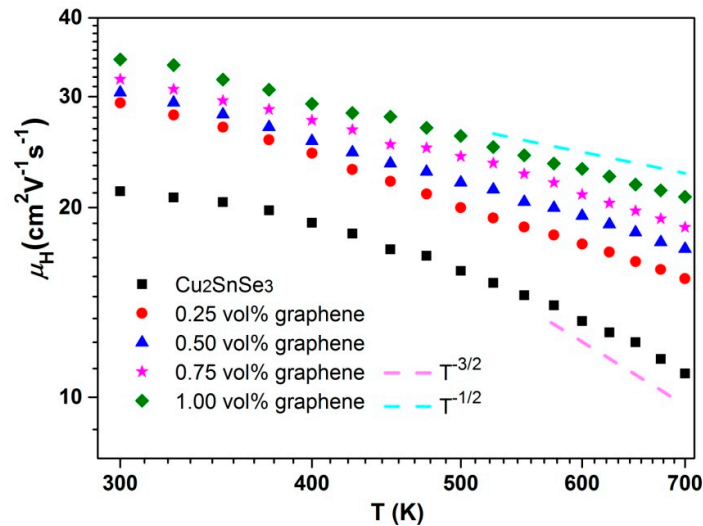


Figure 10. Carrier mobility (μ_{H}) of graphene/ Cu_2SnSe_3 samples as a function of temperature.

Table 1 lists the evaluated equivalent m^* of graphene/ Cu_2SnSe_3 samples at room temperature. Meanwhile, it can also be observed in Figure 10 that the μ_{H} of pristine Cu_2SnSe_3 shows a temperature dependence of $T^{-3/2}$ above 520 K, suggesting that the dominant scattering mechanism is phonon scattering in the temperature range from 520 K to 700 K. Below 520 K, the μ_{H} of pristine Cu_2SnSe_3 proportional to $T^{-3/2}$ is weak, and the relationship of μ_{H} as function of temperature dependence of $T^{-0.5}$ can be seen, showing that alloy scattering is the dominate mechanism in this temperature range. However, the μ_{H} of graphene/ Cu_2SnSe_3 samples deviates from the $T^{-1.5}$ or $T^{-0.5}$ dependence across the entire temperature range, indicating the dominative mechanism is mixed scattering in these composites.

3.3. Thermal Conductivity

The κ and κ_1 for graphene/Cu₂SnSe₃ samples as function of temperature is shown in Figure 11. The κ_1 is obtained by directly subtracting the carrier thermal conductivity κ_c from the total thermal conductivity; κ_c can be calculated according to the Wiedemann–Franz law, $\kappa_c = L_0\sigma T$, where the Lorenz constant L_0 is taken as $2.45 \times 10^{-8} \text{ V}^2/\text{K}^2$. The κ for all composites decreases with the increasing temperature. With the fraction of graphene increasing, the κ of graphene/Cu₂SnSe₃ composites firstly declines then starts to increase. The achieved κ of 0.25% graphene/Cu₂SnSe₃ sample at room temperature is 2.5 W/m·K, which is a 12% reduction from that of pristine Cu₂SnSe₃. On the contrary, the κ of the 1.0% graphene/Cu₂SnSe₃ sample at room temperature increases to 3.45 W/m·K. The κ_1 of graphene/Cu₂SnSe₃ samples demonstrates similar changes compared to that of pure Cu₂SnSe₃. The lowest κ_1 of 0.25% graphene/Cu₂SnSe₃ samples is 0.78 W/m·K, which is 22% lower than that of the pristine Cu₂SnSe₃ sample. As is known to all, nanostructuring will reduce the κ_1 of material as the long-wavelength phonon scattering at grain boundaries was suppressed. Because graphene itself has high lattice thermal conductivity and large specific surface area, an opposite effect of graphene nanosheets on the κ of Cu₂SnSe₃ can be allowed. On one side, the addition of second phase with high κ may increase the total thermal conductivity of composite. On the other side, large specific surface area suggests more newly formed interfaces between the matrix and second phase, which are expected to scatter phonons to depress the κ_1 . For 0.25% graphene/Cu₂SnSe₃, graphene nanosheets are homogeneously dispersed in the Cu₂SnSe₃ matrix, which means the dominative factor should be the influence of interface scattering. By comparison, when the content of graphene exceeds a certain value, the graphene in the composites tends to aggregate into thick flakes in the Cu₂SnSe₃ matrix, as mentioned above. Therefore, the interfacial increment due to the incorporation of graphene should not be significant. This can explain the change in κ_1 of graphene/Cu₂SnSe₃ composites. The results also confirm that the κ_1 of Cu₂SnSe₃ can be effectively reduced by introducing graphene nanosheets. The obtained minimum κ_1 in the present work is 0.78 W/m·K at 700 K for the 1.0% graphene/Cu₂SnSe₃ sample. According to the basic kinetic theory, when the phonon mean free path is equal to the shortest interatomic distance, the lattice thermal conductivity can achieve the minimal value κ_{limin} [32]. The κ_{limin} can be calculated according to the formula $\kappa_1 = 1/3v_m C_V l$, where v_m , C_V , and l are the mean sound velocity, the isochoric specific heat of the system using Dulong and Petit value, and the mean free path of phonon, respectively. The v_m is taken as the constant $2.3 \times 10^3 \text{ m/s}$ [33]. It is assumed that the minimum mean free path of phonon l is the interatomic distance (0.238 nm) of the Cu₂SnSe₃ structure, and the achieved κ_{limin} is $0.52 \text{ W}\cdot\text{m}^{-1}\cdot\text{K}^{-1}$, just as illustrated by the brown dashed line in Figure 11b. By controlling the content of graphene nanosheets and microstructure of composites, the κ_1 of graphene/Cu₂SnSe₃ composites may approach the κ_{limin} of Cu₂SnSe₃ in the high-temperature region. Further optimization will be studied in further work.

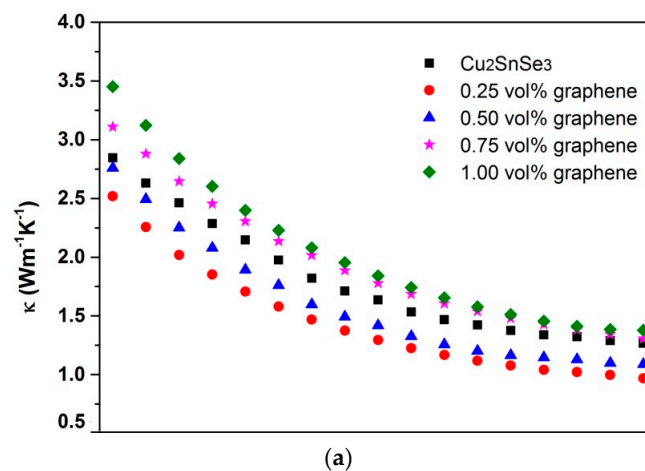


Figure 11. Cont.

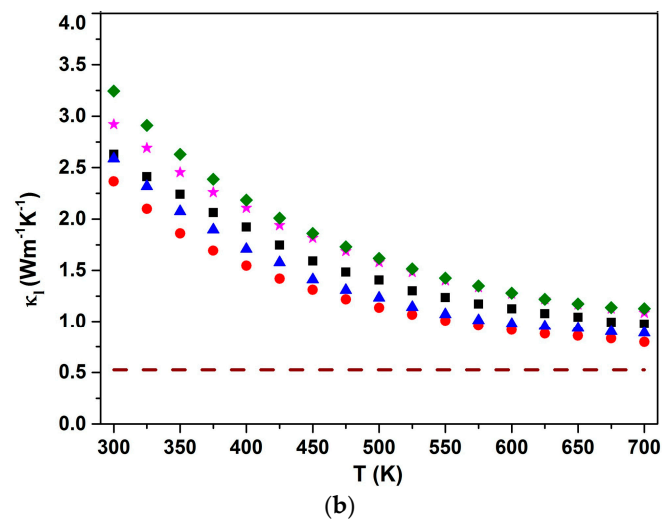


Figure 11. (a) Total thermal conductivity (κ) and (b) lattice thermal conductivity (κ_1) of graphene/ Cu_2SnSe_3 samples as a function of temperature.

3.4. Figure of Merit

Figure 12 shows the ZT value of graphene/ Cu_2SnSe_3 samples as a function of temperature. Like other related Cu-based ternary chalcogenide compounds with diamond-like structure [17,18], the ZT value of graphene/ Cu_2SnSe_3 samples increases with increasing temperature. Compared with the figure of merit of pristine Cu_2SnSe_3 , the ZT of graphene/ Cu_2SnSe_3 samples is obviously improved. The 0.25% graphene/ Cu_2SnSe_3 composite has the maximal ZT value of 0.44 at 700 K, 45% higher than that of pristine Cu_2SnSe_3 . If the graphene/ Cu_2SnSe_3 samples were coated by a coating film and the measured temperature increased to 850 K, the ZT value is capable of reaching 1.0–1.2. The enhancement of ZT for graphene/ Cu_2SnSe_3 composites is basically ascribed to the depressed κ_1 and the increased σ . The incorporation of graphene nanosheets into the Cu_2SnSe_3 could enhance the thermoelectric properties. Therefore, if we choose the material with optimized carrier concentration and mobility as the thermoelectric matrix, the thermoelectric composite with a higher ZT value could be achieved.

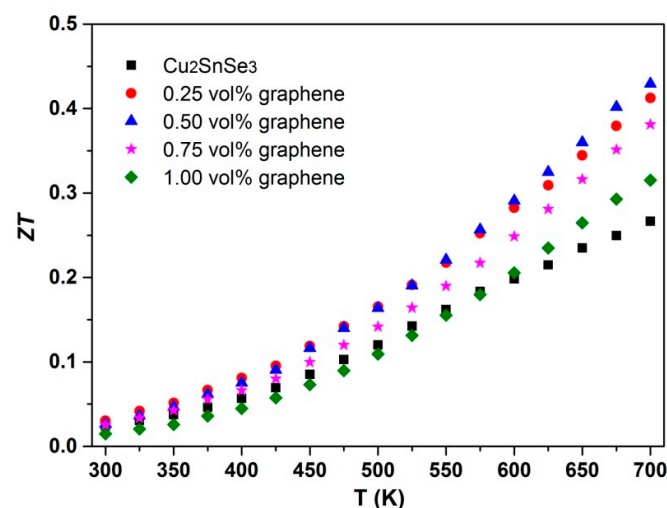


Figure 12. The dimensionless figure of merit of (ZT) of graphene/ Cu_2SnSe_3 samples as a function of temperature.

4. Conclusions

The graphene nanosheets were introduced into the Cu_2SnSe_3 matrix by ball milling and the graphene/ Cu_2SnSe_3 composite was fabricated by spark plasma sintering. The graphene nanosheets distributed uniformly in the Cu_2SnSe_3 matrix. Meanwhile, some graphene nanosheets tended to form thick aggregations and the average length of aggregations was about 3 μm . With the increasing content of graphene, the electrical conductivity of graphene/ Cu_2SnSe_3 samples greatly increased, while the Seebeck coefficient was decreased. The introduction of graphene nanosheets reduced the thermal conductivity, effectively resulting from the phonon scattering by the graphene interface. When the fraction of graphene exceeds a certain value, the thermal conductivity of graphene/ Cu_2SnSe_3 composites starts to increase. The maximum figure of merit ZT for 0.25 vol % graphene/ Cu_2SnSe_3 was 0.44 at 700 K.

Acknowledgments: This work is financially supported by National Natural Science Foundations of China (Grants Nos. 51471076, 51202088).

Author Contributions: All authors participated in the research, analysis and edition of the manuscript. Degang Zhao designed the experiments and Xuezheng Wang fabricated the samples. All authors contributed to the characterization and data analysis. Degang Zhao wrote the paper.

Conflicts of Interest: The authors declare no conflicts of interest.

References

1. Sootsman, J.R.; Chung, D.Y.; Kanatzidis, M.G. New and old concepts in thermoelectric materials. *Angew. Chem. Int. Ed.* **2009**, *48*, 8616–8639. [[CrossRef](#)] [[PubMed](#)]
2. Shi, X.; Chen, L.D.; Uher, C. Recent advance in high-performance bulk thermoelectric materials. *Int. Mater. Rev.* **2016**, *61*, 379–415. [[CrossRef](#)]
3. Gayner, C.; Kar, K.K. Recent advances in thermoelectric materials. *Prog. Mater. Sci.* **2016**, *83*, 330–382. [[CrossRef](#)]
4. Zhao, L.D.; Kanatzidis, M.G. An overview of advanced thermoelectric materials. *J. Materiomics* **2016**, *2*, 101–103. [[CrossRef](#)]
5. Zhou, X.Y.; Wang, G.W.; Guo, L.J.; Chi, H.; Wang, G.Y.; Zhang, Q.F.; Chen, C.Q.; Travis, T.; Jeff, S.; David, V.P. Hierarchically structured TiO_2 for Ba-filled skutterudite with enhanced thermoelectric performance. *J. Mater. Chem. A* **2014**, *2*, 20629–20635. [[CrossRef](#)]
6. Li, G.D.; Baijaj, S.; Aydemir, U.; Hao, S.Q.; Xiao, H.; Goddard, W.A.; Zhai, P.C.; Zhang, Q.J.; Snyder, G.J. P-type Co interstitial defects in thermoelectric skutterudite CoSb_3 due to the breakage of Sb_4 rings. *Chem. Mater.* **2016**, *28*, 2172–2179. [[CrossRef](#)]
7. Gelbstein, Y.; Dashevsky, Z.; Dariel, M.P. In-doped $\text{Pb}_{0.5}\text{Sn}_{0.5}\text{Te}$ p-type samples prepared by powder metallurgical processing for thermoelectric applications. *Physica B* **2007**, *396*, 16–21. [[CrossRef](#)]
8. Gelbstein, Y.; Davidow, J. Highly efficient functional $\text{Ge}_x\text{Pb}_{1-x}\text{Te}$ based thermoelectric alloys. *Phys. Chem. Chem. Phys.* **2014**, *16*, 20120–20126. [[CrossRef](#)] [[PubMed](#)]
9. Gelbstein, Y. Phase morphology effects on the thermoelectric properties of $\text{Pb}_{0.25}\text{Sn}_{0.25}\text{Ge}_{0.5}\text{Te}$. *Acta Mater.* **2013**, *61*, 1499–1507. [[CrossRef](#)]
10. Dado, B.; Gelbstein, Y.; Mogiliansky, D.; Ezersky, V.; Dariel, M.P. Structural evolution following spinodal decomposition of the pseudoternary compound $(\text{Pb}_{0.3}\text{Sn}_{0.1}\text{Ge}_{0.6})\text{Te}$. *J. Electron. Mater.* **2010**, *39*, 2165–2171. [[CrossRef](#)]
11. Kirievsky, K.; Shlimovich, M.; Fuks, D.; Gelbstein, Y. An ab-initio study of the thermoelectric enhancement potential in nano-grained TiNiSn . *Phys. Chem. Chem. Phys.* **2014**, *16*, 20023–20029. [[CrossRef](#)] [[PubMed](#)]
12. Kirievsky, K.; Gelbstein, Y.; Fuks, D. Phase separation and antisite defects possibilities for enhancement the thermoelectric efficiency in TiNiSn half-Heusler alloys. *J. Solid State Chem.* **2013**, *203*, 247–254. [[CrossRef](#)]
13. Sadia, Y.; Dinnerman, L.; Gelbstein, Y. Mechanical Alloying and Spark Plasma Sintering of Higher Manganese Silicides for Thermoelectric Application. *J. Electron. Mater.* **2013**, *42*, 1926–1931. [[CrossRef](#)]

14. Gelbstein, Y.; Tunbridge, J.; Dixon, R.; Reece, M.J.; Ning, H.P.; Gilchrist, R.; Summers, R.; Agote, I.; Lagos, M.A.; Simpson, K.; et al. Physical, mechanical and structural properties of highly efficient nanostructured n- and p-silicides for practical thermoelectric applications. *J. Electron. Mater.* **2014**, *43*, 1703–1711. [[CrossRef](#)]
15. Liu, G.H.; Chen, K.X.; Li, J.T.; Li, Y.Y.; Zhou, M.; Li, L.F. Combustion synthesis of Cu_2SnSe_3 thermoelectric materials. *J. Eur. Ceram. Soc.* **2016**, *36*, 1407–1415. [[CrossRef](#)]
16. Lu, X.; Morelli, D.T. Thermoelectric properties of Mn doped Cu_2SnSe_3 . *J. Electron. Mater.* **2012**, *41*, 1554–1558. [[CrossRef](#)]
17. Shi, X.Y.; Xi, L.L.; Fan, J.; Zhang, W.Q.; Chen, L.D. Cu–Se bond network and thermoelectric compounds with complex diamond like structure. *Chem. Mater.* **2010**, *22*, 6029–6031. [[CrossRef](#)]
18. Fan, J.; Liu, H.L.; Shi, X.Y.; Bai, S.Q.; Shi, X.; Chen, L.D. Investigation of thermoelectric properties of $\text{Cu}_2\text{Ga}_x\text{Sn}_{1-x}\text{Se}_3$ diamond-like compounds by hot pressing and spark plasma sintering. *Acta Mater.* **2013**, *61*, 4297–4304. [[CrossRef](#)]
19. Skoug, E.J.; Cain, J.D.; Morelli, D.T. Thermoelectric properties of the Cu_2SnSe_3 - Cu_2GeSe_3 solid solution. *J. Alloys Compd.* **2012**, *506*, 18–23. [[CrossRef](#)]
20. Bux, S.K.; Fleurial, J.P.; Kaner, R.B. Nanostructured materials for thermoelectric applications. *Chem. Commun.* **2011**, *46*, 8311–8324. [[CrossRef](#)] [[PubMed](#)]
21. Balaya, P. Size effects and nanostructured materials for energy applications. *Energy Environ. Sci.* **2008**, *1*, 645–654. [[CrossRef](#)]
22. Amatya, R.; Ram, R.J. Trend for thermoelectric materials and their earth abundance. *J. Electron. Mater.* **2012**, *41*, 1011–1558. [[CrossRef](#)]
23. Liang, B.B.; Song, Z.J.; Wang, M.H.; Wang, L.J.; Jiang, W. Fabrication and thermoelectric properties of graphene/ Bi_2Te_3 composite materials. *J. Nanomater.* **2013**, *15*, 210767–210772.
24. Kim, J.; Lee, E.S.; Kim, J.Y.; Choi, S.M.; Lee, K.H.; Seo, W.S. Thermoelectric properties of unoxidized graphene/ $\text{Bi}_2\text{Te}_{2.7}\text{Se}_{0.3}$ composites synthesized by exfoliation/re-assembly method. *Phys. Status Solidi (RRL)* **2014**, *8*, 1–5. [[CrossRef](#)]
25. Chen, H.J.; Yang, C.Y.; Liu, H.L.; Zhang, G.H.; Wan, D.Y.; Huang, F.Q. Thermoelectric properties of CuInTe_2 /graphene composites. *CrystEngComm* **2013**, *15*, 6648–6651. [[CrossRef](#)]
26. Feng, B.; Xie, J.; Cao, G.S.; Zhu, T.J.; Zhao, X.B. Enhanced thermoelectric properties of p-type CoSb_3 /graphene nanocomposite. *J. Mater. Chem. A* **2013**, *1*, 13111–13119. [[CrossRef](#)]
27. Faleev, S.V.; Leonard, F. Theory of enhancement of thermoelectric properties of materials with nano-inclusions. *Phys. Rev. B* **2008**, *77*, 214304. [[CrossRef](#)]
28. Zebajadi, M.; Esfarjani, K.; Shakouri, A.; Zeng, G.; Lu, H.; Zide, J.; Gossard, A. Effect of nanoparticle scattering on thermoelectric power factor. *Appl. Phys. Lett.* **2009**, *94*, 202105. [[CrossRef](#)]
29. Dong, J.D.; Liu, W.; Li, H.; Su, X.L.; Tang, X.F.; Uher, C. In situ synthesis and thermoelectric properties of PbTe -graphene nanocomposites by utilizing a facile and novel wet chemical method. *J. Mater. Chem. A* **2013**, *1*, 12503–12511. [[CrossRef](#)]
30. Gharleghi, A.; Liu, Y.F.; Zhou, M.H.; He, J.; Tritt, T.M.; Liu, C.J. Enhancing the thermoelectric performance of nanosized CoSb_3 via short-range percolation of electrically conductive WTe_2 inclusions. *J. Mater. Chem. A* **2016**, *4*, 13874–13879. [[CrossRef](#)]
31. Ortiz, B.R.; Crawford, C.M.; McKinney, R.W.; Parilla, P.A.; Toberer, E.S. Thermoelectric properties of bromine filled CoSb_3 skutterudite. *J. Mater. Chem. A* **2016**, *4*, 8444–8449. [[CrossRef](#)]
32. Morelli, D.T.; Jovovic, V.; Heremans, J.P. Intrinsically minimal thermal conductivity in cubic I-V-VI₂ semiconductors. *Phys. Rev. Lett.* **2008**, *101*, 035901. [[CrossRef](#)] [[PubMed](#)]
33. Cho, J.Y.; Shi, X.; Salvador, J.R.; Meisner, G.P. Thermoelectric properties and investigations of low thermal conductivity in Ga-doped Cu_2GeSe_3 . *Phys. Rev. B* **2011**, *84*, 085207. [[CrossRef](#)]

